Do Oyster Colonies Influence Sediment Erodibility? A Hydro-morphodynamic Characterization of Intertidal Estuarine Reefs by Way of Jet Erosion Test and Acoustic Doppler Current Profiler

Melody Thomas[1], Joanna Quiah[2], Celso F. Castro-Bolinaga[2], Grace Massey[3], Steve Hall[2], Nina Stark[4], and Samuel Consolvo[4]

[1]Department of Biological and Agricultural Engineering, North Carolina State University, Raleigh, NC 27695, USA; e-mail: mathoma6@ncsu.edu Corresponding author.
[2]Deparement of Biological and Agricultural Engineering, North Carolina State University, Raleigh, NC 27695, USA; e-mail: jquiah@ncsu.edu, cfcastro@ncsu.edu, shall5@ncsu.edu
[3]Department of Physical Sciences, Virginia Institute of Marine Sciences, Gloucester Point, VA 23062, USA; e-mail: grace.massey@vims.edu
[4]Department of Civil and Environmental Engineering, Virginia Tech, Blacksburg, VA 24061, USA; e-mail: ninas@vt.edu, samueltc@vt.edu

ABSTRACT

Estuaries provide a unique habitat for shellfish species in a constantly changing environment. These species provide crucial ecosystem services, including mitigating the effects of eutrophication and providing habitat for other species. The objective of this work was to investigate the effects that oyster colonies have on sediment erodibility in an estuarine environment. This paper presents the results of a hydro-morphodynamic characterization of three intertidal reefs located at the Rachel Carson Research Reserve, NC, USA, one that is exposed to moderate flow conditions (U = 0.07 m/s, where U is the median depth-averaged flow velocity) where the bed material is silty sand with a large among of oyster fragments and shells, and two that are exposed to more pronounced flow conditions (U = 0.20 m/s) where the bed material is poorly graded sand with a reduced presence of oyster fragments and shells. Critical shear stress (τ_c) and erodibility coefficient (k_d), collectively known as erodibility parameters, were determine in-situ via the Jet Erosion Test, and the depth-averaged characteristics of the flow field were measured using an Acoustic Doppler Current Profiler. At the intertidal reef exposed to moderate flow conditions, the presence of oyster colonies appears to influence the erodibility parameters, resulting in higher values of τ_c and lower values of k_d in locations close to the oysters than in locations further away from the reef. Moreover, at the intertidal reefs that are exposed to more pronounced flow conditions, the variability of τ_c in locations surrounding the reef is less significant but the magnitude of k_d does change, suggesting that the presence of the oyster reef primarily affects the rate of sediment movement once the threshold for motion has been exceeded. It was also noted that in all locations the presence of fragmented oysters and shells significantly increases τ_c, independently of the acting flow condition. Although the evaluated reefs represent a limited variety of environmental conditions, preliminary results suggest that oyster colonies can indeed impact sediment resistance to erosion.

INTRODUCTION

There is a growing need for advancements and inter-disciplinary collaboration in the field of erosion and scour mitigation as seashores become increasingly vulnerable to sea-level rise.

Coastal erosion causes about $500 million annually in damages and loss of land, and the U.S. spends $150 million annually on shoreline erosion mitigation (NOAA 2013). Although major research efforts have been made in predicting scour dimensions, most methods over-predict scour depths (Falcone and Stark 2016), resulting in scour mitigation designs that are usually expensive and negatively affect the environment around the structure.

Bivalves such as oysters provide physical protection as natural breakwaters (Campbell and Hall 2018), along with providing environmental benefits through filtration and habitat creation (Rodriquez et al. 2014). These natural organisms have been used as bio-stabilizers to enhance sediment cohesiveness and reduce hydrodynamic forces, ultimately decreasing erosion (Udhayakumar and Karande 1989; Widdows and Brinsley 2002; Morris et al. 2019). Moreover, the growth and survival of oysters also affect the dissipation of the flow's turbulent energy. Morris et al. (2019) indicated that for similar hydrodynamic conditions, reefs with healthy oysters dissipate more energy than reefs with no live oysters. The degree of dissipation influences sediment transport dynamics around the reefs, in addition to oyster density and the reef's length to width ratio (Morris et al., 2019). The health of oyster habitats, therefore, is significantly dependent on local-scale hydrodynamics, which at the same time dictate the spatial and temporal scales associated with the surrounding sediment movement.

The objective of this work was to investigate the effects that oyster colonies have on sediment erodibility. This paper examines the results of a hydro-morphodynamic characterization that was performed on three intertidal oyster reefs located at the Rachel Carson Research Reserve, North Carolina, USA. The Jet Erosion Test (JET) (Hanson and Cook 1997, 2004) was used to estimate in-situ critical shear stress (τ_c) and erodibility coefficient (k_d), which are collectively known as erodibility parameters. Additionally, an Acoustic Doppler Current Profiler (ADCP) was deployed to measure the depth-averaged flow velocity, which in turn was used to estimate the applied boundary shear stress (τ_o). Comparison of applied (τ_o) to resisting (τ_c, k_d) forces at the three selected sites suggests that oyster colonies do impact sediment resistance to erosion, primarily by changing its detachment rate once the threshold for motion has been exceeded.

STUDY AREA

The Rachel Carson Reserve (Figure 1a) is located across the historic Town of Beaufort, North Carolina, USA, and it is managed by the NC Coastal Reserve and National Estuarine Research Reserve as part of the Division of Coastal Management from the Department of Environmental Quality. The Reserve is home to a diverse array of coastal habitats (NCDEQ, 2019), and its unique location provides an ideal environment for nesting and breeding of species accustomed to the brackish water of estuaries (EPA 2016). It consists of several islands that are interconnected by shoals and channels that move water and sediment around the area, and it has been designated and protected for the primary purpose of education and research.

Three sites with intertidal oyster reefs were selected for this study: Site 1 located towards the western end of the Reserve (N 34° 42.725' W 076° 40.420'), and Sites 2 and 3 located towards the eastern end (N 34° 42.198' W 076° 37.873' and N 34° 42.155' W 076° 37.800', respectively) (Figure 1a). At a larger scale, these sites were selected to capture different flow and sediment characteristics. The oyster reef in Site 1 was located nearly parallel to the flow, exposed to moderate flow conditions, and the bed material was silty sand (d_{50} = 0.20 mm, where d_{50} is the median grain size) with 7.5-15% of fines (<0.075 mm) and a large amount of oyster fragments and shells. In Sites 2 and 3, the oyster reefs were directly exposed to more pronounced flow conditions,

and the bed material was poorly graded sand (d_{50} = 0.17-0.37 mm)with less than 5% of fines (<0.075mm) and a reduced presence of oyster fragments and shells.

Figure 1 Plan view of (a) the Rachel Carson Reserve and the selected oyster reefs, (b) Site 1 sampling locations, and (c) Sites 2 and 3 sampling locations (Imagery from Google Earth).

Furthermore, within each site, various sampling locations were selected to account for different positions relative to the oyster reefs. In Site 1 (Figure 1b), a total of six (6) locations were tested, three (3) in Site 1A, two (2) in Site 1B, and one (1) in Site 1C. In Site 2 (Figure 1c), four (4) locations were tested, and lastly, in Site 3 (Figure 1c), five (5) locations were tested, two (2) in Site 3A, one (1) in Site 3B, and two (2) in Site 3C.

METHODOLOGY

Flow field characteristics were measured during high tide using a boat-mounted Teledyne 1200 kHz RiverPro Acoustic Doppler Current Profiler (ADCP). Moving-vessel ADCP measurements (e.g., Petrie et al. 2013) were performed to obtain estimates of depth-averaged flow velocities at three (3) transects in Site 1, and at seven (7) transects in Sites 2 and 3. Data were collected using Water Mode 12 and Bottom Mode 5 with a bin size of 0.05 m for all measurements in this study. Data were first analyzed using the WinRiverII Software Version 2.18 (Teledyne RD Instruments, Inc.), and then post-processed to obtain magnitude and direction of depth-averaged velocities using a MATLAB code developed at the Virginia Institute of Marine Sciences. It should be noted that the use of depth-averaged values is because the oyster reefs were located toward the end of the transects, making it difficult to obtain reliable measurements of the velocity profile in relatively shallow flow depths.

Estimates of the depth-averaged flow velocity were then used to compute an averaged value of τ_o per transect. The equation for the logarithmic law of the wall for flow over rough boundaries integrated over the water column (Chang, 1988) was used to compute τ_o as:

$$\tau_0 = \rho \left(\frac{U_i}{\frac{1}{k} * \ln\left(\frac{H_i}{k_s}\right) + 6} \right)^2 \quad (1)$$

where ρ = density of saltwater = 1,021 kg/m^3, U = depth-averaged velocity, k = von Karman Constant = 0.4, H = flow depth, and k_s = characteristics roughness. Herein, the characteristic roughness was assumed to be described by d_{50} for each site as a simplified representation of the bed material to contrast with the results from the in-situ Jet Erosion Test. To compute τ_o, U was first calculated for each ensemble, which is defined as a single recorded measurement of velocity profile (Petrie et al., 2013). Equation 1 was then applied to calculate a value of τ_o per ensemble, thereby allowing for the computation of an average value of τ_o per transect.

Erodibility parameters (τ_c, k_d) were estimated at the selected sites and sampling locations using the Jet Erosion Test (JET) (Hanson and Cook 1997, 2004). During the test, sediment at each sampling location was progressively scoured by a submerged, impinging jet of water that generated $\tau_o > \tau_c$. The temporal variation of the scour hole was recorded throughout the test by measuring the scour depth along the jet centerline. The test continued until the scour hole reached a state of quasi-equilibrium, in which the scour depth did not vary significantly with time. A mini-JET device (Khanal et al., 2016) was used in this study. The height of the constant head tank that drives τ_o was adjusted at each sampling location based on preliminary assessments of the bed material composition. Lastly, analytical methods based on the excess shear stress equation were used to derive the sediment erodibility parameters at each location. Specifically, the Blaisdell Method was applied to estimate τ_c and k_d (Blaisdell et al. 1981; Hanson and Cook 1997, 2004).

RESULTS AND DISCUSSION

The direction of the measured depth-averaged velocities for the surveyed transects at Site 1 is shown in Figure 2a. Therein, the velocity measurements were processed by removing invalid data points and averaging values every two ensembles. Likewise, the magnitude variability of the measured depth-averaged velocities per transect at Site 1 is shown in Figure 2b. Results indicate that the sampling locations are exposed to similar and moderate flow conditions, with median values of U = 7.4 cm/s for transect 1, U = 6.4 cm/s for transect 2, and U = 6.6 cm/s for transect 3. Using Equation 1, transect-averaged values of τ_o are estimated as τ_o = 0.05 Pa for transect 1, and τ_o = 0.03 Pa for transects 2 and 3. It should be noted that these values of τ_o are not the highest that sampling locations at Site 1 would be exposed to. The highest τ_o will correspond to the transition between high tide and ebb/flood conditions. However, the measurements were performed during high tide to ensure that the sampling locations were underwater, thereby allowing the successful deployment of the ADCP.

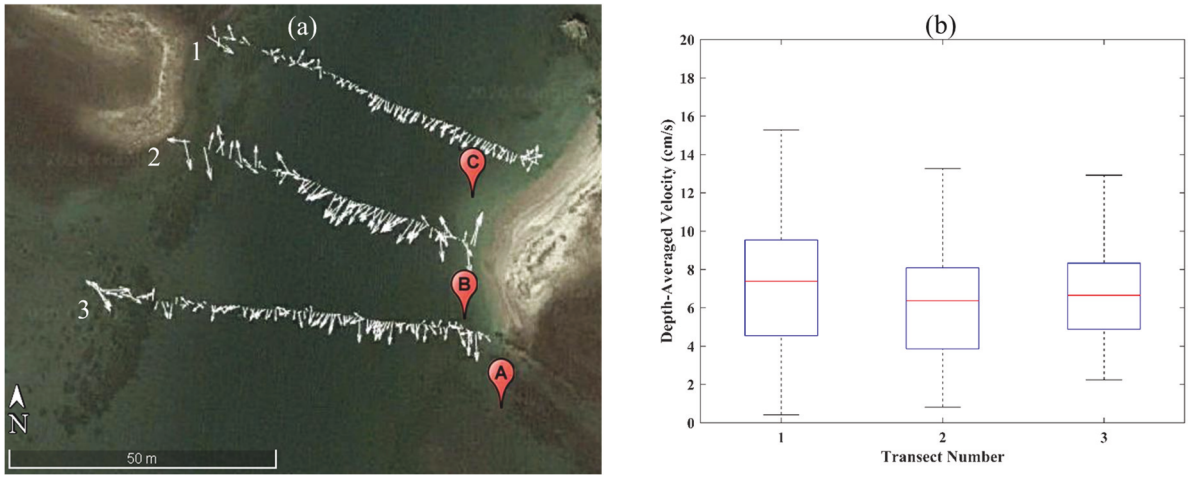

Figure 2 (a) Direction of the depth-averaged velocity for the surveyed transects at Site 1 (Imagery Source Google Earth), and (b) variability of the depth-averaged velocity per surveyed transect at Site 1.

Similarly, the direction and the magnitude variability of the measured depth-averaged velocity for the surveyed transects at Sites 2 and 3 are shown in Figures 3a and 3b, respectively. Therein, the velocity measurements are presented at every ensemble after removing invalid data points. When compared to Site 1, results indicate that the sampling locations are exposed to more pronounced flow conditions, with median values of U ranging from 17.8 cm/s to 23.3 cm/s for Site 2 (transects 3 and 4), and between 14.8 cm/s to 21.9 cm/s for site 3 (transects 5 and 6). The median values of U for each transect are presented in Table 1, as well as the transect-averaged values of τ_o estimated using Equation 1. Results also show an increase in τ_o when compared to Site 1. In this case, the measurements were also performed during high tide to ensure that the sampling locations were underwater, thereby allowing the successful deployment of the ADCP. Although the spatial variability of the flow velocity (Figures 2a and 3a) is lost when averaging over the entire transect, reported median values of U and transect-averaged τ_o capture the different flow characteristics measured at the sites.

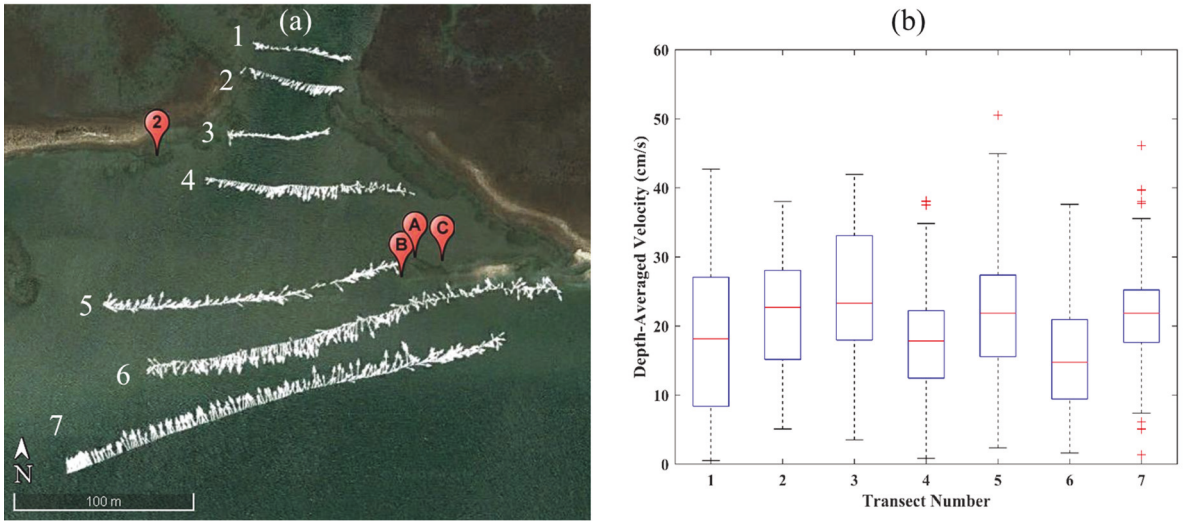

Figure 3 (a) Direction of the depth-averaged velocity for the surveyed transects at Sites 2 and 3 (Imagery Source Google Earth), and (b) variability of the depth-averaged velocity per surveyed transect at Sites 2 and 3.

Table 1 Median values of the depth-averaged velocities and transect-averaged values of the applied boundary shear stress for the surveyed transects at Sites 2 and 3.

Transect	1	2	3	4	5	6	7
U_{median} (cm/s)	18.1	22.7	23.3	17.8	21.9	14.8	21.8
τ_o (Pa)	0.33	0.39	0.52	0.33	0.57	0.35	0.43

JET-derived erodibility parameters for all sampling locations at Site 1 are presented in Table 2. To enhance the analysis of the results, d_{50}, % fines (<0.075 mm), and τ_c estimated using the Shields diagram (hereafter referred to as $\tau_{c\text{-Shields}}$) are also included. Sampling locations A1, A2, and A3 (N 34° 42.417' W 076° 40.397') represent high, medium, and low oyster density areas. Sampling locations B1 and B2 (N 34° 42.726' W 076° 40.400') correspond to sites in the perimeter of the oyster reef, whereas location C1 (N 34° 42.738' W 76° 40.399') is far from and not influenced by the reef. Results indicate that τ_c is higher at sampling locations within the oyster reef, and that it progressively decreases as the distance from the reef increases, reaching a similar value to $\tau_{c\text{-Shields}}$ at location C1. The increase in τ_c is likely due to the significant amount of oyster fragments and shells present in bed material within the reef. At location A, results indicate that τ_c is similar for areas with high, medium, and low oyster density, but that k_d is lower for the high-density area, implying that the rate of sediment detachment is lower once $\tau_o > \tau_c$. Moreover, k_d remains low and similar at both peripheral locations B1 and B2, and it significantly increases at location C1, consistent with the relatively low grain-sized dominated τ_c. The sediment detachment behavior measured during the JET is shown in Figure 4 by the relationship between the erosion rate (ε_r) and τ_o. Therein, linear fits are illustrated with the intent of highlighting the general direction of the trend. However, laboratory tests have shown that this relationship does not always follow a linear behavior (Wardinski et al., 2018). Figure 4a clearly shows a lower detachment rate for location A1 (high-density oyster area) as revealed by the slope of the linear fit, and Figure 4c illustrates the high erosion rates that were measured at location C1 for relatively low values of τ_o.

Table 2 JET-derived erodibility parameters for sampling locations at Site 1. Bed material median grain size, % fines, and critical shear stress from the Shield's diagram are also shown.

Location	τ_c (Pa)	k_d (cm^3/N·s)	d_{50} (mm)	% Fines (<0.075 mm)	$\tau_{c\text{-Shields}}$ (Pa)
A1	1.93	3.35	0.21	15.0	0.16
A2	1.43	7.63	0.21	7.5	0.16
A3	2.62	7.78	0.20	< 5.0	0.16
B1	0.41	5.03	1.16	15.0	0.65
B2	0.21	5.33	0.23	< 5.0	0.18
C1	0.12	42.05	0.35	< 5.0	0.22

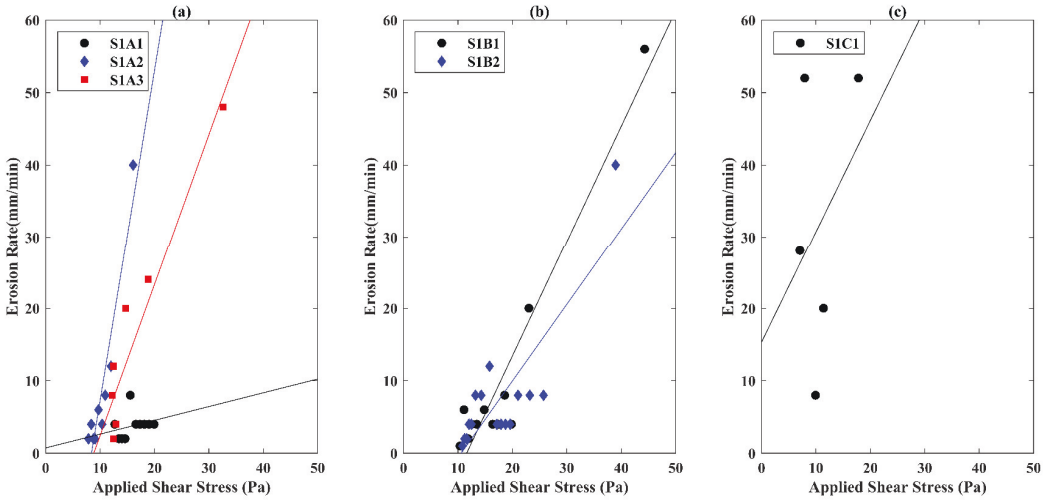

Figure 4 Relationship between erosion rate and applied boundary shear stress at Site 1 for sampling locations (a) A, (b) B, and (c) C. Linear fit is shown to highlight general direction of trend measured during the Jet Erosion Test.

Similarly, JET-derived erodibility parameters, d_{50}, and $\tau_{c\text{-Shields}}$ for sampling locations at Site 2 (N 34° 42.194' W 76° 37.894') are presented in Table 3. Sampling locations A1 and A2 correspond to areas behind the oyster reefs and toward the island. Location A3 is situated in an area surrounded by the oyster reef, and location A4 correspond to a region in in front of the reef that is directly exposed to the flow. When compared to Site 1, the variability of τ_c appears to be less significant at Site 2. Important differences between these sites are the reduced amount of oyster fragments and shells, and the smaller % fines (<0.075 mm) in the bed material, which can be attributed to the effects of moderate versus more pronounced local flow conditions. Therefore, τ_c seems to more influenced by the grain size of the sediment than by the presence of the reef, as revealed by the magnitudes of d_{50} and $\tau_{c\text{-Shields}}$. At site 2, results suggest that the oyster reef primarily affects the sediment detachment rate. Table 3 indicates that the location directly exposed to the flow has the highest k_d (location A4), and that the region surrounded by the oyster reef has the lower value of k_d (location A3). Moreover, both areas behind the reef have similar values of k_d (locations A1 and A2). Figure 5 graphically illustrates this behavior by showing the relationship between ε_r and τ_o during the JET. The variation clearly shows that higher values of τ_o are needed to generate the similar magnitudes of ε_r at location A3 when compared to location A4. The variation also shows intermediate detachment rates for locations A1 and A2. Additional research is needed to understand the specific processes (e.g., biological factors and/or oyster's by-products) that drive the observed spatial variability of k_d relative to the location of the oyster reef.

Table 3 JET-derived erodibility parameters for sampling locations at Site 2. Bed material median grain size, % fines, and critical shear stress from the Shield's diagram are also shown.

Location	$\tau_{c\text{-JET}}$ (Pa)	k_d (cm^3/N·s)	d_{50} (mm)	% Fines (<0.075 mm)	$\tau_{c\text{-Shields}}$ (Pa)
A1	0.06	10.76	0.18	< 5.0	0.16
A2	1.53	9.8	0.18	< 5.0	0.16
A3	0.58	2.73	0.20	< 5.0	0.16
A4	1.24	23.92	0.22	< 5.0	0.17

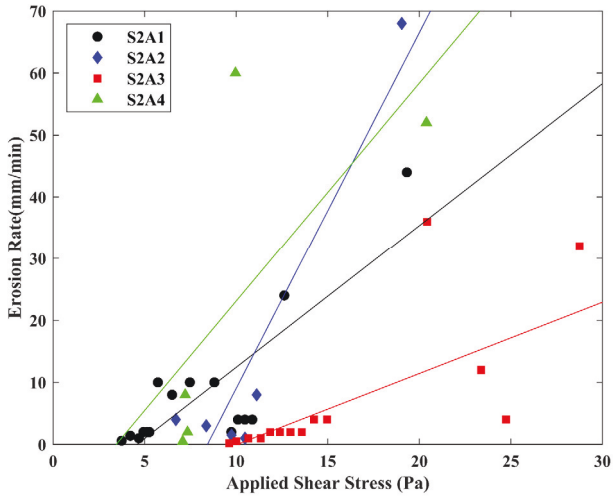

Figure 5 Relationship between erosion rate and applied boundary shear stress for sampling locations at Site 2. Linear fit is shown to highlight general direction of trend measured during the Jet Erosion Test.

Table 4 presents the JET-derived erodibility parameters, d_{50}, and $\tau_{c\text{-Shields}}$ for all sampling locations at Site 3. Sampling locations A1 and A2 (N 34° 42.163' W 76° 37.799') correspond to areas behind and toward the western end of the oyster reef. Location B1 (N 34° 42.157' W 76° 37.804') is placed at the western end of the reef and directly exposed to the flow, and locations C1 and C2 (N 34° 42.162' W 76° 37.789') correspond to a region behind and toward the eastern end of the reef. Overall, results indicate that τ_c was relatively low and k_d relatively high, except for locations A1 and B1. In these two areas, a significant amount of oyster fragments and shells was present in the bed material, particularly in location B1. When compared to Site 2, one importance difference is that the reef was mainly composed of oysters that were not alive. Results suggest that this may have an impact on the magnitude of k_d, as τ_c seems to more influenced by either the density of oyster fragments and shells or the grain size of the sediment. Moreover, the relationship between ε_r and τ_o illustrated in Figure 6 supports the high values of k_d, indicating rather high values of ε_r that were measured relative to the magnitude of τ_o. Figure 6 also shows the impact of the large amount of oyster fragments and shells at location B1.

Table 4 JET-derived erodibility parameters for sampling locations at Site 3. Bed material median grain size and critical shear stress calculated from the Shield's diagram are also shown.

Location	τ_c (Pa)	k_d (cm^3/N·s)	d_{50} (mm)	% Fines (<0.075 mm)	$\tau_{c\text{-Shields}}$ (Pa)
A1	2.17	80.13	0.17	< 5.0	0.16
A2	0.01	21.87	0.20	< 5.0	0.16
B1	9.11	3.35	0.37	< 5.0	0.21
C1	1.10	61.77	0.17	5.4	0.16
C2	0.15	37.23	0.18	< 5.0	0.16

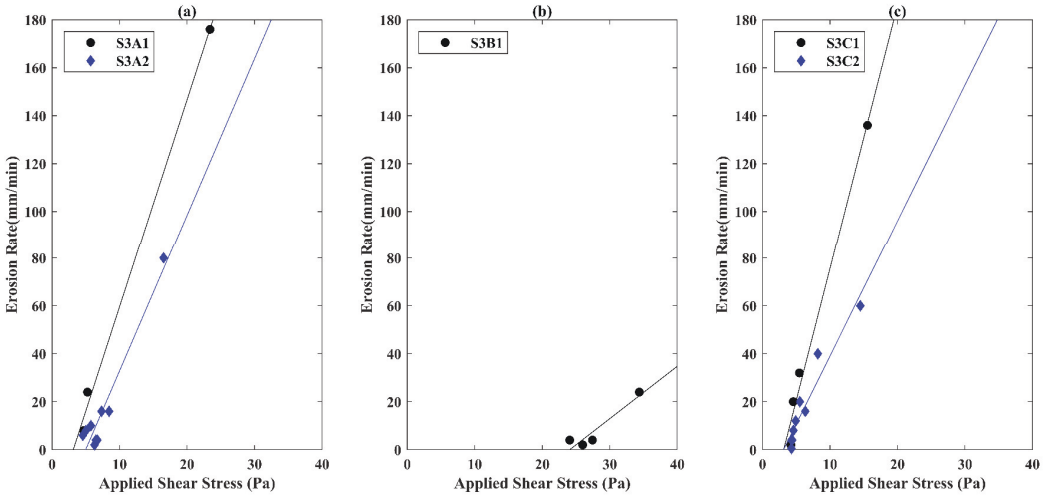

Figure 6 Relationship between erosion rate and applied boundary shear stress at Site 3 for sampling locations (a) A, (b) B, and (c) C. Linear fit is shown to highlight general direction of trend measured during the Jet Erosion Test.

CONCLUDING REMARKS

The following concluding remarks were developed based on the results of a hydro-morphodynamic characterization of three intertidal oyster reefs at the Rachel Carson Research Reserve, North Carolina, USA:

1. Comparison of applied to resisting forces suggests that τ_c is more influenced by the presence of oyster reefs at sites with moderate flow conditions than at sites exposed to more pronounced flow conditions.
2. The magnitude of τ_c significantly increases if a large amount of oyster fragments and shells are present in the bed material, independently of the acting flow condition. Moreover, observations suggest that the acting flow condition in turn affect the amount of oyster fragments and shells, and the percent of fines in the bed material.
3. At sites with more pronounced flow conditions and with a reduced amount of oyster fragments and shells in the bed material, τ_c seems to be more influenced by the bed material grain size with the presence of the oyster reef primarily affecting the magnitude of k_d.

Subsequent data collection is underway to address the impacts of a more detailed sediment characterization. Additional research is needed to understand the influence of biological processes (e.g., by-products produced by the oysters) that may influence the spatial variability of erodibility parameters at and around oyster reefs.

ACKNOWLEDGEMENTS

This project was funded by the National Science Foundation through grants CMMI-1820848 and CMMI-1820842. This work was also supported by the USDA National Institute of Food and Agriculture Hatch Project 1016113. The authors would also like to thank Brandon Puckett and Paula Gillikin for assistance with field work.

REFERENCES

Blaisdell, F. W., Hebaus, G. G., & Anderson, C. L. (1981). Ultimate dimensions of local scour. Journal of the Hydraulics Division, 107(3), 327-337.

Campbell, M. D., & Hall, S. G. (2018). Hydrodynamic effects on oyster aquaculture systems: A review. Reviews in Aquaculture, 11(3), 896-906. doi:10.1111/raq.12271

Chang, H.H., 1988. Fluvial Processes in River Engineering. Krieger Publishing Company, Malabar, Florida.

Environmental Protection Agency (EPA). (2016). "Basic Information about Estuaries." Environmental Protection Agency, www.epa.gov/nep/basic-information-about-estuaries.

Falcone Jr., F. T., & Stark, N. (2016). Evaluation of the performance of scour prediction equations with regards to flow and sediment characteristics. Paper presented at the Geo-Chicago 2016, 671-680.

Hanson, G. J., & Cook, K. R. (1997). Development of excess shear stress parameters for circular jet testing. ASAE Paper, 972227.

Hanson, G. J., & Cook, K. R. (2004). Apparatus, test procedures, and analytical methods to measure soil erodibility in situ. Applied engineering in agriculture, 20(4), 455.

Khanal, A., Fox, G.A., & Al-Madhhachi, A.T. (2016). Variability of Erodibility Parameters from Laboratory Mini Jet Erosion Tests. Journal of Hydrologic Engineering, 21(10), 04016030.

Morris, R. L., Bilkovic, D. M., Boswell, M. K., Bushek, D., Cebrian, J., Goff, J., . . . Swearer, S. E. (2019). The application of oyster reefs in shoreline protection: Are we over-engineering for an ecosystem engineer? Journal of Applied Ecology, 56(7), 1703-1711. doi:10.1111/1365-2664.13390.

North Carolina Department of Environmental Quality (NCDEQ). (2014). "NC Coastal Reserve and National Estuarine Research Reserve: Research, Education, and Management Materials." portal.ncdenr.org/web/crp/publications1.

National Oceanic and Atmospheric Administration (NOAA). (2013). "Beach Nourishment: A Guide for Local Government Officials. https://coast.noaa.gov/archived/beachnourishment/html/human/law/index.htm

Petrie, J., Diplas, P., Gutierrez, M., & Nam, S. (2013). Combining fixed- and moving-vessel acoustic doppler current profiler measurements for improved characterization of the mean flow in a natural river. Water Resources Research, 49(9), 5600-5614. doi:10.1002/wrcr.20396

Rodriguez, A. B., Fodrie, F. J., Ridge, J. T., Lindquist, N. L., Theuerkauf, E. J., Coleman, S. E., Grabowski, J.H., Brodeur, M.C., Gittman, R.K., Keller, D.A., & Kenworthy, M. D. (2014). Oyster reefs can outpace sea-level rise. Nature Climate Change, 4(6), 493-497. doi:10.1038/nclimate2216

Udhayakumar, M., & Karande, A. A. (1989). Byssal threads of Mytilopsis sallei (recluz) and their adhesive strength. Proceedings: Animal Sciences, 98, 65-76. doi:10.1007/BF03179566.

Wardinski, K.M., Guartault, L., Fox, G.A., & Castro-Bolinaga, C.F. (2018). Suitability of a Linear Model for Predicting Cohesive Soil Detachment during Jet Erosion Tests. Journal of Hydraulic Engineering, 23(9): 06018004.

Widdows, J., & Brinsley, M. (2002). Impact of biotic and abiotic processes on sediment dynamics and the consequences to the structure and functioning of the intertidal zone. Journal of Sea Research, 48(2), 143-156. doi:10.1016/S1385-1101(02)00148-X